Dominique Pêcheur,[1] *Florence Lefebvre,*[1] *Arthur T. Motta,*[2] *Clément Lemaignan,*[1] *and Daniel Charquet*[3]

Oxidation of Intermetallic Precipitates in Zircaloy-4: Impact of Irradiation

REFERENCE: Pêcheur, D., Lefebvre, F., Motta, A. T., Lemaignan, C., and Charquet, D., **"Oxidation of Intermetallic Precipitates in Zircaloy-4: Impact of Irradiation,"** *Zirconium in the Nuclear Industry: Tenth International Symposium, ASTM STP 1245,* A. M. Garde and E. R. Bradley, Eds., American Society for Testing and Materials, Philadelphia, 1994, pp. 687–708.

ABSTRACT: Intermetallic precipitates are known to play a critical role in the oxidation process of Zircaloys. Since under irradiation they undergo structural changes, a specific study was conducted to analyze whether these transformations modify the oxidation behavior of the Zircaloy-4. Oxidation kinetics in autoclave were measured on reference, ion irradiated, and neutron irradiated materials. In the case of ion-irradiated samples, the oxidation kinetics are changed, while in the case of neutron-irradiated cladding, no significant change is observed after 60 days of oxidation. The behavior of reference and irradiated precipitates during the growth of these oxide layers was analyzed using analytical scanning transmission electron microscopy. Close to the metal-oxide interface, precipitates are incorporated unoxidized in the oxide layer. Then, when oxidized, at a few hundreds of nanometers from this interface, they undergo two major evolutions: their structure becomes either nanocrystalline or occasionally amorphous and an iron redistribution and depletion is observed. In the case of precipitates previously made amorphous by irradiation, a similar behavior is observed. The role of precipitates on the oxidation of the Zircaloy-4 is discussed in terms of interaction of the precipitates with the zirconia layer (stability of the dense oxide layer) and oxidation kinetics.

KEY WORDS: zirconium, precipitates, oxidation, oxide layer, oxidation kinetics, zirconia, irradiation, amorphization, analytical scanning transmission electron microscopy, zirconium alloys, nuclear materials, nuclear applications, radiation effects

In light water reactor (LWR) conditions, the oxidation of Zircaloy cladding is one of the main limitations to the extension of fuel rod burnups.

Many studies were conducted to evaluate the oxidation process in autoclave environments. The oxidation kinetics are generally divided in two main regions separated by a transition [*1*]. During the first one, called the pre-transition region, the oxide that is formed is dense, is composed of monoclinic and tetragonal ZrO_2 crystallites, and the growth rate decreases continuously. After the transition, the oxidation rate increases and remains approximately constant in the second stage. Most of the outer part of the oxide layer is now porous [*2,3*] and composed exclusively of monoclinic ZrO_2 crystallites [*4*]. Several metallurgical parameters greatly influence the oxidation kinetics. Among them, the influence of the nature and the

[1] Research engineers and head of Laboratory, respectively, CEA-Grenoble, DTP/SECC, 85X, 38041 Grenoble Cedex, France.

[2] Assistant professor, Pennsylvania State University, Department of Nuclear Engineering, University Park, PA 16802.

[3] Research engineer, Cézus, Centre de Recherches d'Ugine, 74340 Ugine, France.

distribution of intermetallic precipitates on oxidation is clearly established, but the origin of such an effect is not well understood [*5–7*].

However, these results concerning the oxidation kinetics of Zircaloys in autoclave environments cannot be transferred to reactor environments where a significant increase of the oxidation rate is measured when the oxide thickness exceeds a few microns [*8,9*]. To understand such an effect, various approaches are proposed based on the differences of the chemical environment in-reactor and in-autoclave [*10*] or on the radiolysis phenomena within pores [*11,12*]. Since it is known that precipitates in Zircaloys play a significant role in the oxidation process and because precipitates evolve under irradiation [*13–18*], it is important to evaluate the effect of the irradiation-induced amorphization of the precipitates on the oxidation kinetics.

The oxidation rates of reference, ion-irradiated, and neutron-irradiated materials were therefore measured in the autoclave to separate the effect of chemical reactor environments from those of radiation damage in the cladding. Several oxide layers grown on reference and ion-irradiated materials have been characterized by transmission electron microscopy (TEM). Some have already been described [*19*]. In addition, new observations on thicker oxides are briefly summarized to introduce local oxygen analysis. The oxide layer formed in-reactor on a three-cycle irradiated cladding sample was described. These observations were discussed, and particular attention are paid to determine the role of intermetallic precipitates on oxidation kinetics.

Experimental Methods

Materials

The reference material used in this work is standard Zircaloy-4 (Zy4 STD) furnished by Cézus of Ugine, France. Samples were machined out of a 1-mm-thick plate (Zr-1.48Sn-0.21Fe-0.11Cr-0.10O) and fully recrystallized at 948 K for 3 h and 30 min after cold rolling ($\Sigma Ai = 4 \cdot 10^{-19}$ h using $Q/R = 40\,000$ K). To increase precipitate size and thereby facilitate their observation, some specimens of the standard Zircaloy-4 were subjected to an additional coarsening heat treatment at 1055 K for 50 h. This material with large precipitates is referred to as Zy4 HT. Some samples (20 by 30 mm) have been irradiated on both faces with 1.5 MeV He^+ ion irradiations in the Van de Graaff ion accelerator of the Centre d'Etudes Nucléaires de Grenoble, at 77 K and to a dose of 0.4 displacements per atom (dpa), to simulate neutron irradiation and produce, at the surface, amorphous precipitates. Details of the irradiation conditions are described elsewhere [*19,20*].

Reference and irradiated recrystallized Zircaloy-4 cladding materials have also been used in this work. The chemical compositions of these materials are Zr-1.75Sn-0.23Fe-0.10Cr-0.11O and Zr-1.71Sn-0.21Fe-0.12Cr-0.15O, respectively. The irradiated cladding samples (25-mm-long tubes) were exposed to two and three irradiation cycles in the experimental BR3 reactor at about 590 K to fluences of 4.0 and 5.4 10^{25} n $\cdot$ m^{-2}, respectively. The oxide thickness produced during three cycles has been estimated, when preparing thin foils, to be of the order of 10 μm.

Oxidation and Examinations

Reference and ion-irradiated samples were oxidized in autoclave (10.3 MPa steam, 673 K). The neutron-irradiated samples, before being oxidized, were mechanically polished to remove the oxide layer grown in-reactor whereas their internal surface remained as-received. The neutron-irradiated and reference cladding samples were oxidized together in a shielded auto-

clave (15 MPa steam, 673 K). After 60 days of oxidation, three samples were removed for metallographic examinations while the autoclave testing of other specimens continued.

Oxide layers formed in-autoclave and in-reactor were examined using JEOL 1200 EX and a TOPCON 002B 200 kV scanning transmission electron microscopes. Compositions were determined by energy dispersive X-ray spectroscopy. This foils were prepared from the specimen regions at the metal-oxide interface, in the middle of the oxide layer and at the oxide-water interface. The experimental method used for preparing these thin foils has been described in Refs *19* and *20*. In the case of neutron-irradiated materials, the same method was used within a shielded cell.

In order to follow the evolution of precipitates from the very beginning of their incorporation into the dense oxide layer to their complete stabilization in the porous oxide layer, different thicknesses of oxide were grown in-autoclave and characterized as 1, 2, 4, and 14 μm (that is, 3, 20, 40, and 420 days of oxidation, respectively) in the case of reference materials and 1, 2, and 10 μm (that is, 3, 20, and 120 days of oxidation, respectively) in the case of ion-irradiated materials. In the case of the neutron-irradiated materials, thin foils have been prepared in the middle of the oxide layer grown in-reactor for three cycles.

Experimental results

Oxidation of Reference and Irradiated Zircaloy-4

Oxidation kinetics obtained on reference and ion-irradiated Zircaloy-4 are presented in Fig. 1. The ion-irradiated material exhibits a higher oxidation rate than the reference one. This increase is particularly significant for Zy4 HT irradiated to a dose of 0.4 dpa once the oxide thickness is greater than 3 μm. Surprisingly, this increase of the oxidation rate is maintained even after the irradiation-damaged surface layer is consumed by the autoclave oxidation process. In the case of standard material irradiated at 0.6 dpa, a spalling of the oxide occurs after 60 to 80 days of oxidation.

In the case of neutron-irradiated cladding, after 60 days of autoclave oxidation, different behaviors are observed on the inside and outside tube surfaces. No significant differences in oxide thicknesses exist between the external surfaces of the irradiated material and the reference unirradiated specimen. In both cases, the thickness of the external oxide layer ranges between 2 and 3 μm. On the other hand, the internal surface of the cladding samples irradiated for 2 and 3 cycles exhibited a much thicker oxide layer (≈15 μm) than the reference specimens (≈2 μm) (Fig. 2). Moreover, this thick oxide layer presented cracks with a tendency to spalling.

Oxidation of Reference $Zr(Fe,Cr)_2$ precipitates

The precipitates present in the Zircaloy-4 sheet used in this work are mainly $Zr(Fe,Cr)_2$ Laves phases with both C14 hcp and C15 fcc crystalline structure and an iron/chromium ratio close to 1.7. In the case of Zy4 STD, their average diameter is equal to about 130 nm while in Zy4 HT, it is close to 330 nm.

In the Dense Oxide Layer—At a few hundred nanometers away from the metal-oxide interface, unoxidized and oxidized precipitates are found. The unoxidized ones have the same crystalline structure (hcp or fcc) and the same iron/chromium (Fe/Cr) ratio (1.7) as in the precipitates in the metallic matrix, and no oxygen is detected (Fig. 3). The oxidized precipitates are composed of nanocrystallites, a few nanometers in size. Their structure, identified by

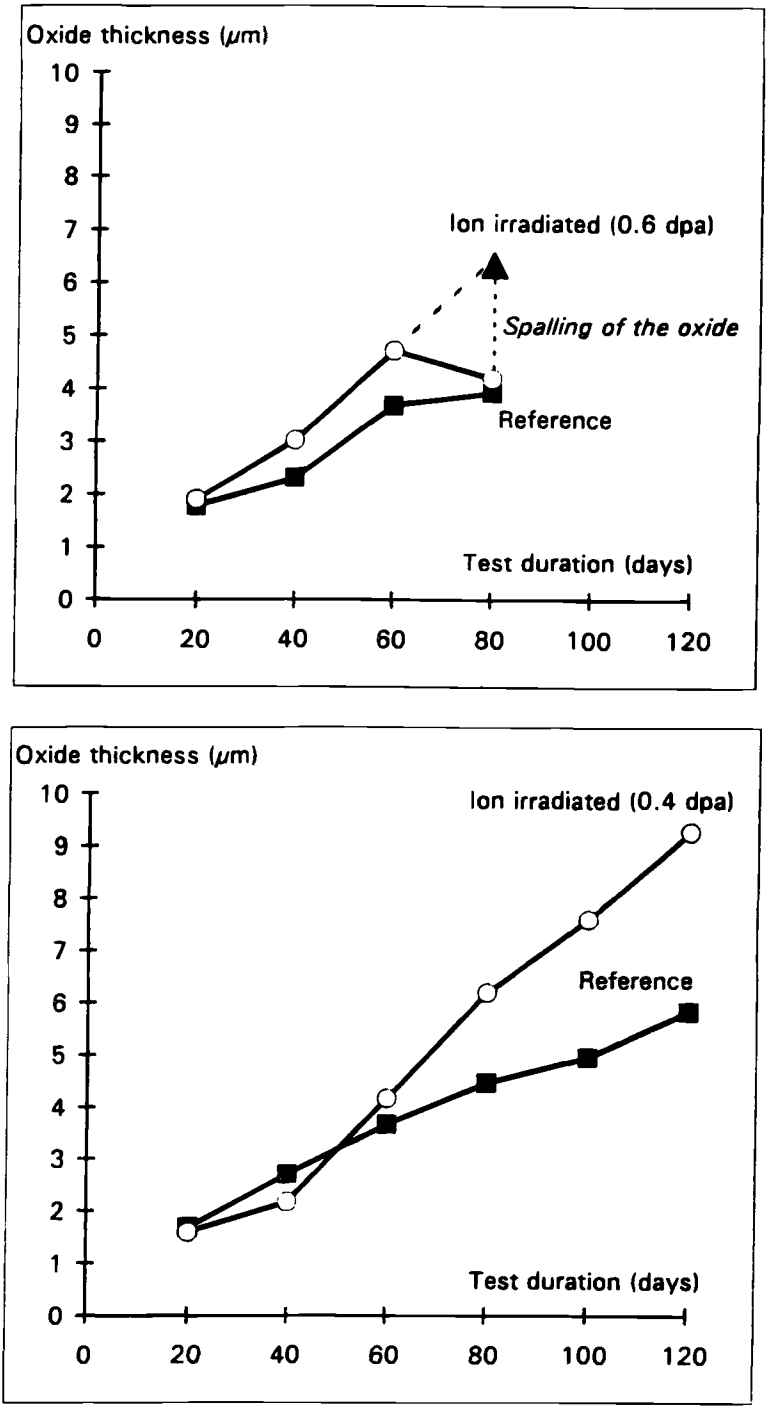

FIG. 1—*Oxidation kinetics in a 15 MPa steam test autoclave of reference and ion-irradiated Zircaloy-4 at 400°C:* (top) *Zy4 STD with normal precipitates, and* (bottom) *Zy4 HT with large precipitates.*

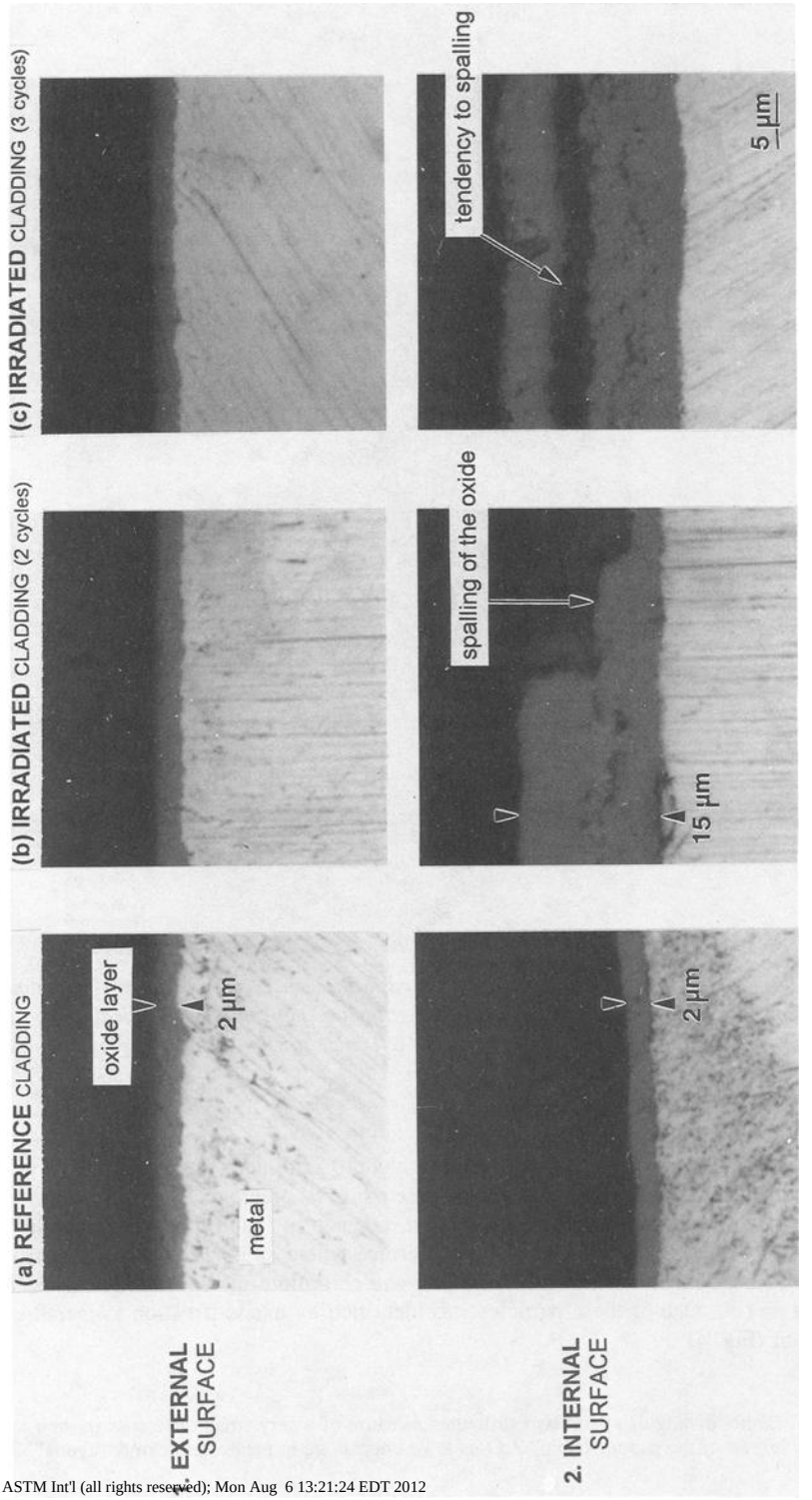

FIG. 2—*Oxide layers formed, in shielded autoclave after 60 days of oxidation, (1) on the external surface and (2) on the internal surface of:* (a) *a reference cladding,* (b) *two cycles of neutron-irradiated cladding, and* (c) *three cycles of neutron-irradiated cladding.*

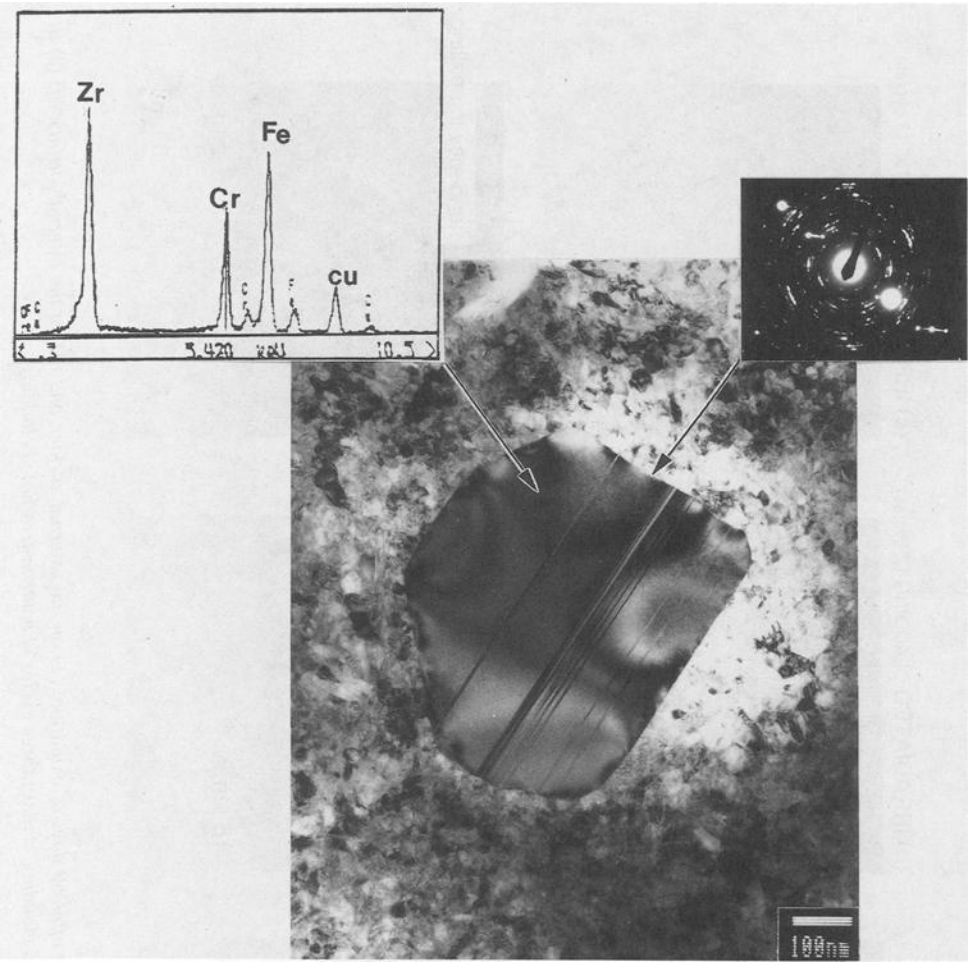

FIG. 3—*Unoxidized Zr(Fe,Cr)$_2$ precipitate observed in the dense oxide layer at a few hundred nanometers from the metal-oxide interface. Both its structure (hcp) and its chemical composition (Fe/Cr ≈ 1.7) are similar to those observed for the reference precipitates present in the metallic matrix.*

electronic diffraction, corresponds to cubic (or tetragonal)[4] ZrO_2 with small amounts of monoclinic ZrO_2. Chemical composition analysis of these oxidized precipitates shows a Fe/Cr ratio smaller than 1.7 indicating a slight iron depletion. Oxygen is found throughout precipitates except, occasionally, at the precipitate-matrix interface where small particles, a few tens of nanometers in size, composed exclusively of iron and chromium in the metallic state can be found (Fe/Cr ≈ 1.5). One of these particles was identified by nanodiffraction as metallic bcc iron-chromium (Fig. 4).

[4] Since TEM cannot distinguish these two structures, because of a very small difference in their lattice parameters, in the rest of the paper, "cubic" ZrO_2 is to be understood to mean "cubic or tetragonal" ZrO_2.

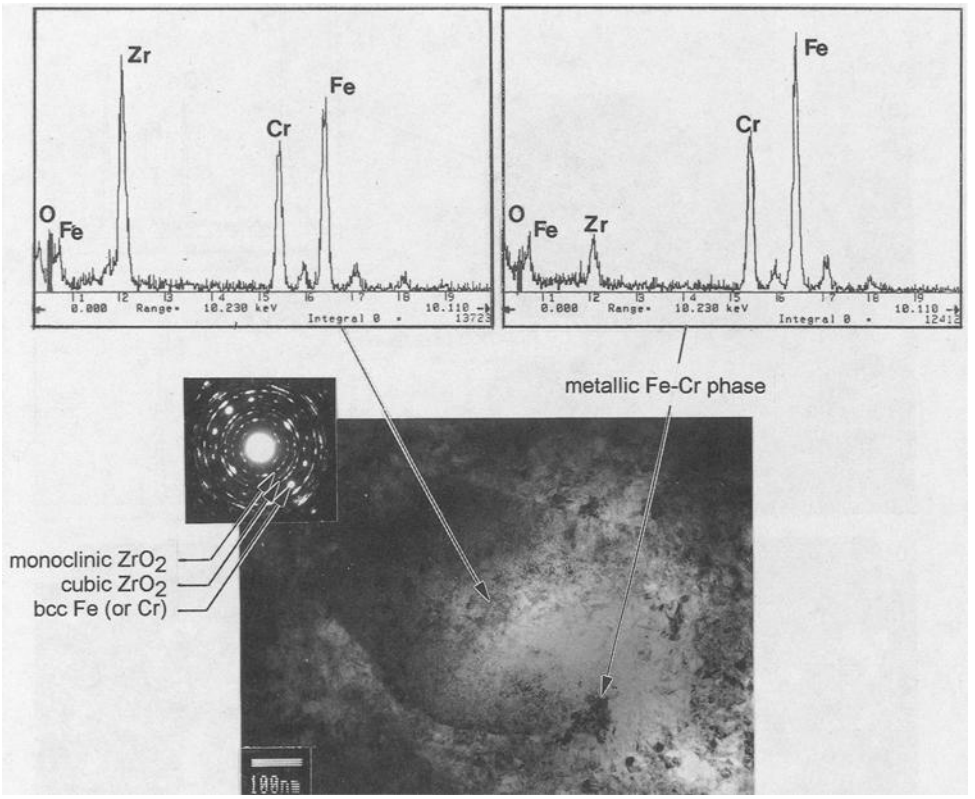

FIG. 4—*Oxidized precipitate observed in the dense oxide layer at a few hundred nanometers from the metal-oxide interface. It is composed of nanocrystallites of cubic and monoclinic ZrO_2 and, at the edge of the precipitate, of a bcc iron-chromium phase with no trace of oxygen. Only minor evolution of the Fe/Cr ratio is observed with respect to the reference precipitates (Fe/Cr > 1).*

At about 1 μm away from the metal-oxide interface, in the dense oxide layer, all precipitates are observed to be nanocristallized and oxidized except a few amorphous ones [*19*]. Nanocrystallized precipitates have the same structure as described earlier, but their chemical composition has considerably changed (Fig. 5). Their Fe/Cr ratio is now decreased to less than 1 and some iron is segregated at the edges of the precipitates. This segregation occasionally corresponds to metallic bcc iron. Only a small percentage of chromium is found in it (Fe/Cr > 3).

In the Porous Oxide Layer—At a few microns or a few tens of microns away from the metal-oxide interface, all the precipitates observed are nanocrystallized and oxidized. Their crystalline structure has not changed nor has their chemical composition (cubic ZrO_2, Fe/Cr < 1). Nanocrystallites within precipitates remain small (a few nanometers in size) compared to those observed in the surrounding matrix (a few tens of nanometers). However, the metallic iron-rich bcc phase is no longer observed, indicating an iron dissolution into the matrix.

These observations are summarized in Fig. 6. Close to the metal-oxide interface, the precipitates are incorporated, unoxidized, in the oxide layer implying that they oxidize later than the

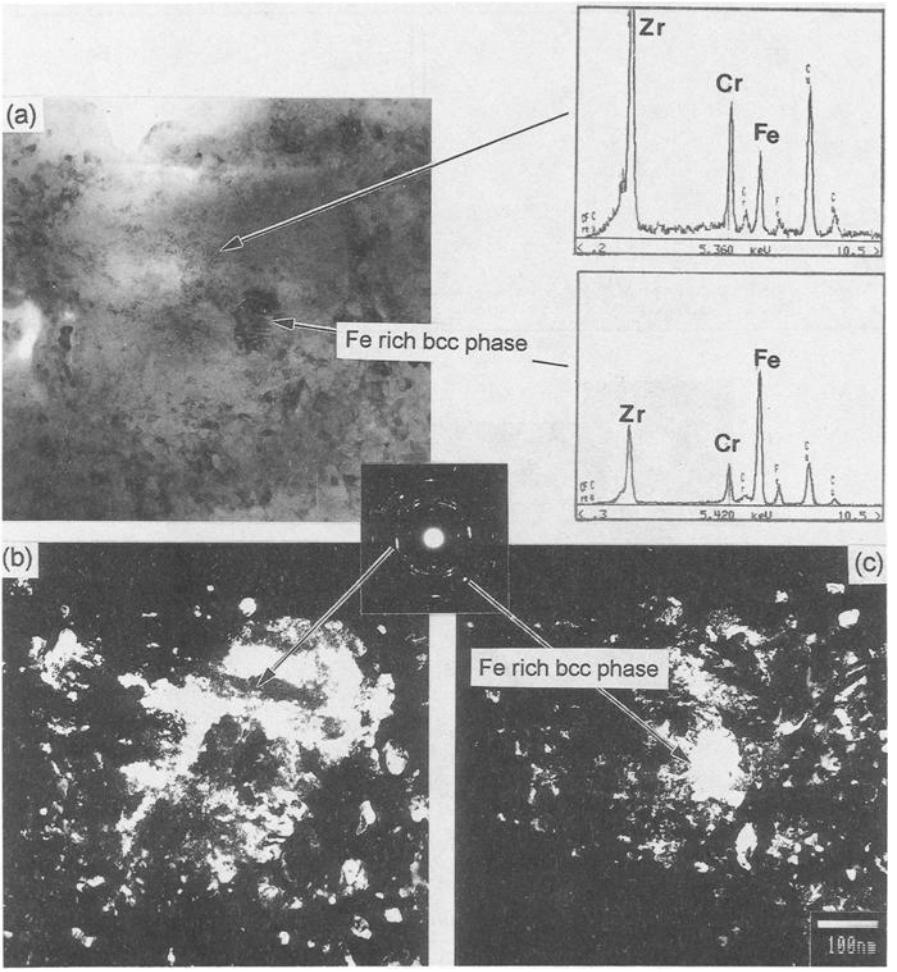

FIG. 5—*(a) Oxidized precipitate observed in the dense oxide layer, at about one micron from the metal-oxide interface,* (b) *a dark field from the oxide rings shows it is still composed of nanocrystallites of cubic and monoclinic* ZrO_2, *and* (c) *a bcc iron and chromium phase is also detected. The Fe/Cr ratio of the precipitate is now decreased to less than one and the bcc phase is now richer in iron.*

zirconium matrix. When oxidized, they are composed essentially of nanocrystallites of cubic ZrO_2. During their oxidation, they undergo a drastic iron redistribution leading to an iron depletion that is more pronounced in the middle of the precipitates and occasionally to a metallic iron precipitation at the edges of the precipitates. Finally, the iron partially dissolves in the ZrO_2 matrix. These results are valid for both Zy4 STD and HT.

Oxidation of Irradiated $Zr(Fe,Cr)_2$ Precipitates

Ion-Irradiated Precipitates—The 1.5 MeV He, ion-irradiated Zircaloy-4 samples present amorphous $Zr(Fe,Cr)_2$ precipitates within a few microns of the surface. Their nearest neighbor

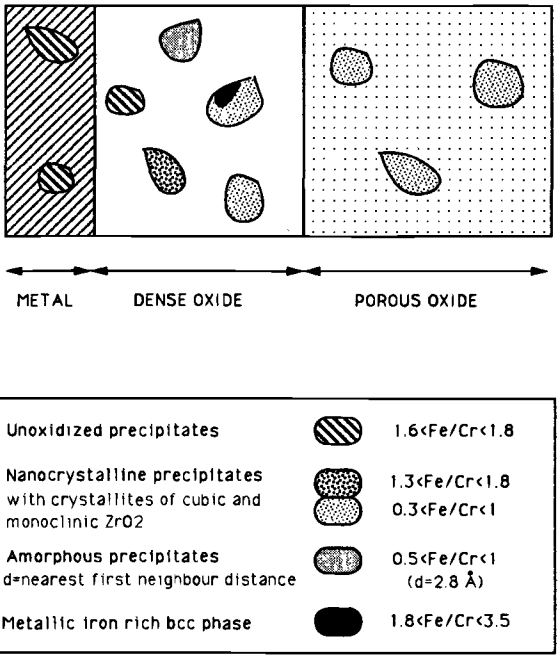

FIG. 6—*Schematic view of the structural and chemical composition evolutions experienced by the reference Zr(Fe,Cr)$_2$ precipitates during their incorporation in the Zircaloy-4 oxide layer grown in-reactor.*

spacing is equal to 2.2 Å. As previously reported [*21*], the chemistry of these precipitates amorphized by ion irradiation has not changed (Fe/Cr ≈ 1.7).

In the dense oxide layer—At a few hundred nanometers away from the metal-oxide interface, both amorphous and nanocrystallized precipitates are observed. Amorphous precipitates have a nearest neighbor spacing ranging between 2.2 and 2.8 Å and nanocrystallized precipitates are composed of ZrO_2 cubic and monoclinic crystallites. Both have a Fe/Cr ratio close to 1.5, indicating a slight iron depletion. At about 1 μm away from the metal-oxide interface, in the dense oxide layer, both amorphous (Fig. 7) and nanocrystallized precipitates (Fig. 8) are still observed. The amorphous precipitates, usually the smallest (<450 nm), are characterized by a nearest neighbor spacing close to 2.8 Å (for 2.2 Å before oxidation). Concurrently, oxygen is detected in these amorphous precipitates and their Fe/Cr ratio is decreased to about 0.5. Metallic bcc phases composed of iron (≈90%) and chromium (≈10%) are observed at the edges of some of these precipitates.

The nanocrystallized oxidized precipitates, composed of cubic and monoclinic ZrO_2 crystallites, have a higher Fe/Cr ratio (1.5) and are usually larger than amorphous ones. They also occasionally present a metallic bcc iron-chromium external layer.

In the porous oxide layer—At a few microns away from the metal-oxide interface, amorphous and nanocrystallized precipitates are present. Their structures are similar to those just described, and their Fe/Cr ratio is close to 0.3. No iron-rich metallic bcc phases are found in this outer layer.

The results are summarized in Fig. 9: when incorporated in the oxide layer, the irradiated precipitates behave similar to the reference ones. They experience structural and chemical

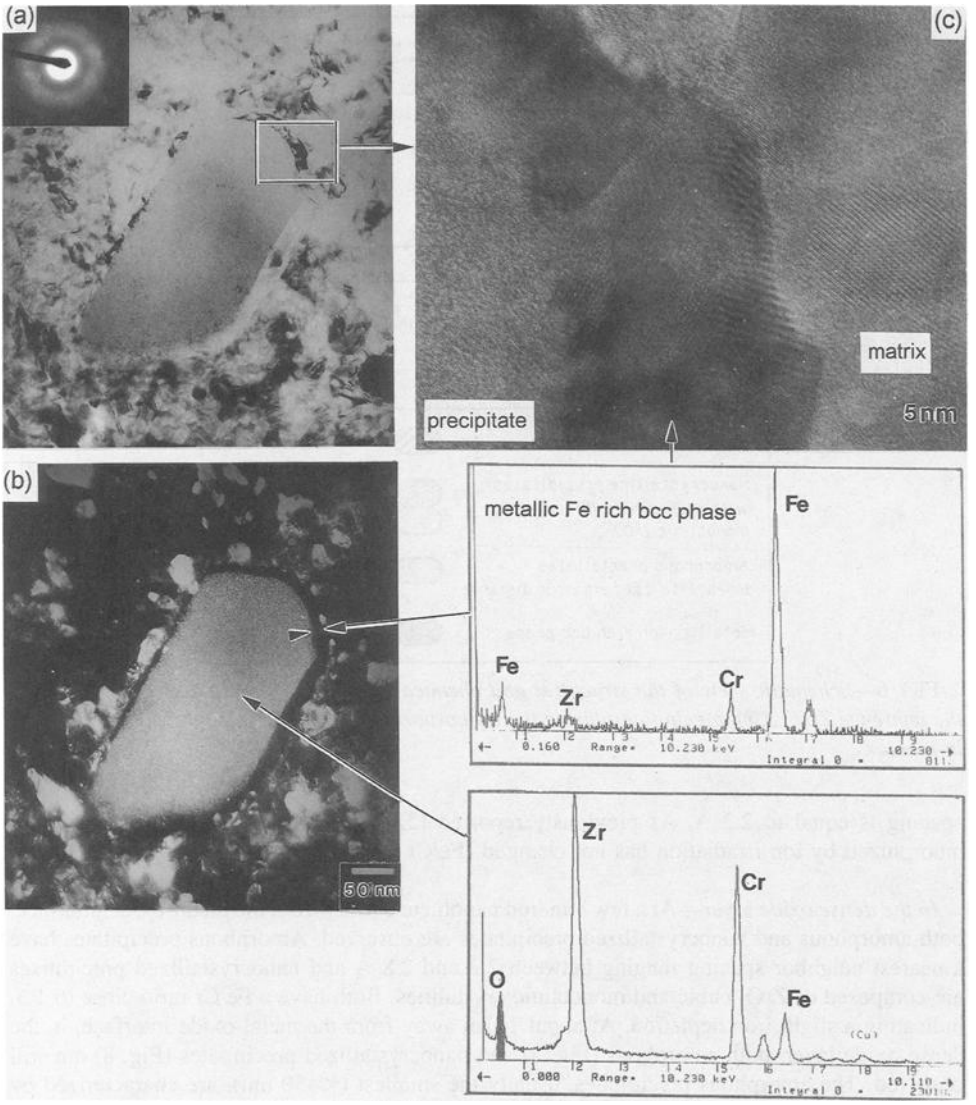

FIG. 7—*Ion-irradiated precipitate observed in the dense oxide layer at about one micron from the metal-oxide interface.* (a) *It is still amorphous but its first neighbor distance has increased during the oxidation process from 2.2 to 2.8 Å and its Fe/Cr ratio has decreased to less than 1,* (b) *a metallic iron-rich bcc phase with no trace of oxygen is observed surrounding the precipitate, and* (c) *high-resolution image of the precipitate-matrix interface.*

changes. Small precipitates (<450 nm) remain amorphous, but their nearest neighbor spacing increases during oxidation (from 2.2 to 2.8 Å) while incorporating oxygen. The largest precipitates become nanocrystallized with cubic ZrO_2 and a small amount of monoclinic ZrO_2. Both undergo a large amount of iron redistribution and depletion, occasionally with a transient metallic iron precipitation, and finally the iron partially dissolves in the ZrO_2 matrix.

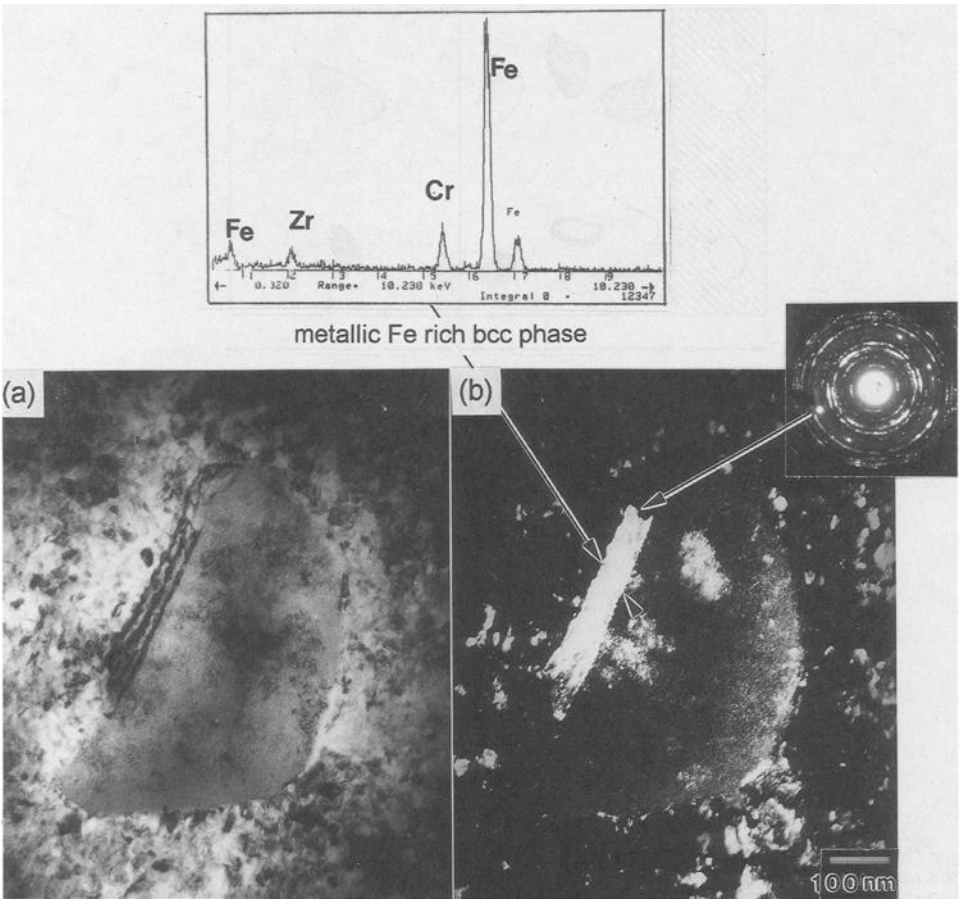

FIG. 8—*Ion-irradiated precipitate observed in the dense oxide layer at about one micron from the metal-oxide interface.* (a) *It is oxidized and composed of nanocrystallites of cubic and monoclinic* ZrO_2 *and* (b) *an iron-rich bcc phase, with no trace of oxygen, is detected at the edge of this precipitate.*

Neutron-Irradiated Precipitates—The state of the precipitates that were present in the cladding materials irradiated for two and three cycles were extensively described in Ref *17*. In the metallic matrix, the $Zr(Fe,Cr)_2$ precipitates experience an amorphous transformation and an iron depletion leading to a progressive dissolution of these precipitates into the matrix. After two cycles, all the precipitates are either amorphous or partially amorphous. Their size is significantly decreased compared to the reference cladding. After three cycles, all are amorphous and their sizes decreased further. The nearest neighbor spacing of these amorphous precipitates is equal to 2.2 Å.

To analyze these precipitates in the oxide layer, thin foils were prepared in the middle of the oxide layer grown in reactor during three cycles of irradiation. All the precipitates observed are completely amorphous with a nearest neighbor spacing equal to 2.7 Å and a Fe/Cr ratio close to 0.6 (Fig. 10). The initial average precipitate size has not changed, indicating that they were incorporated into the oxide before being dissolved into the metallic matrix. However, since those precipitates were incorporated in the oxide layer before the third irradiation cycle,

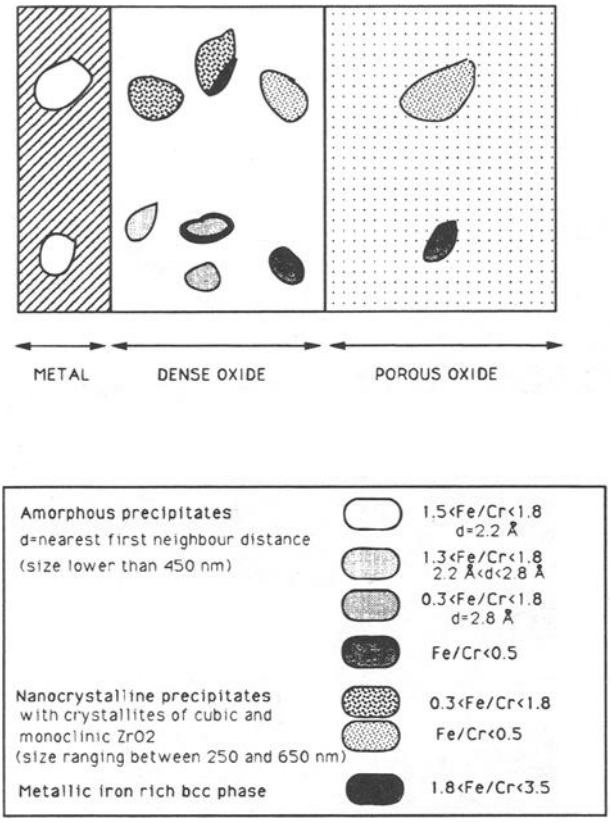

FIG. 9—*Schematic view of the structural and chemical composition evolutions experienced by the ion-irradiated amorphous $Zr(Fe,Cr)_2$ precipitates during their incorporation in the Zircaloy-4 oxide layer formed in-autoclave.*

at a time when they may have been only partially amorphous, it is impossible to determine if they became fully amorphous before being oxidized or during the oxidation process. The observation of thin foils prepared at the metal-oxide interface and at the water-oxide interface, currently in progress, will give us critical information with respect to this point.

Discussion

Oxidation Mechanism of Intermetallic Precipitates

During the precipitate oxidation process, three different steps can be discussed:

1. In the porous oxide layer and in the outermost part of the dense oxide layer, all precipitates are oxidized; whereas, close to the metal-oxide interface, a large number of them remain in their original crystalline structure. The oxidation of intermetallic precipitates is delayed compared to the zirconium matrix. This observation is in good agreement with those previously reported in Zircaloy-2 and -4 [*22,23*]. Moreover, at the beginning of precipitate oxidation, some bcc iron (and chromium) is found indicating

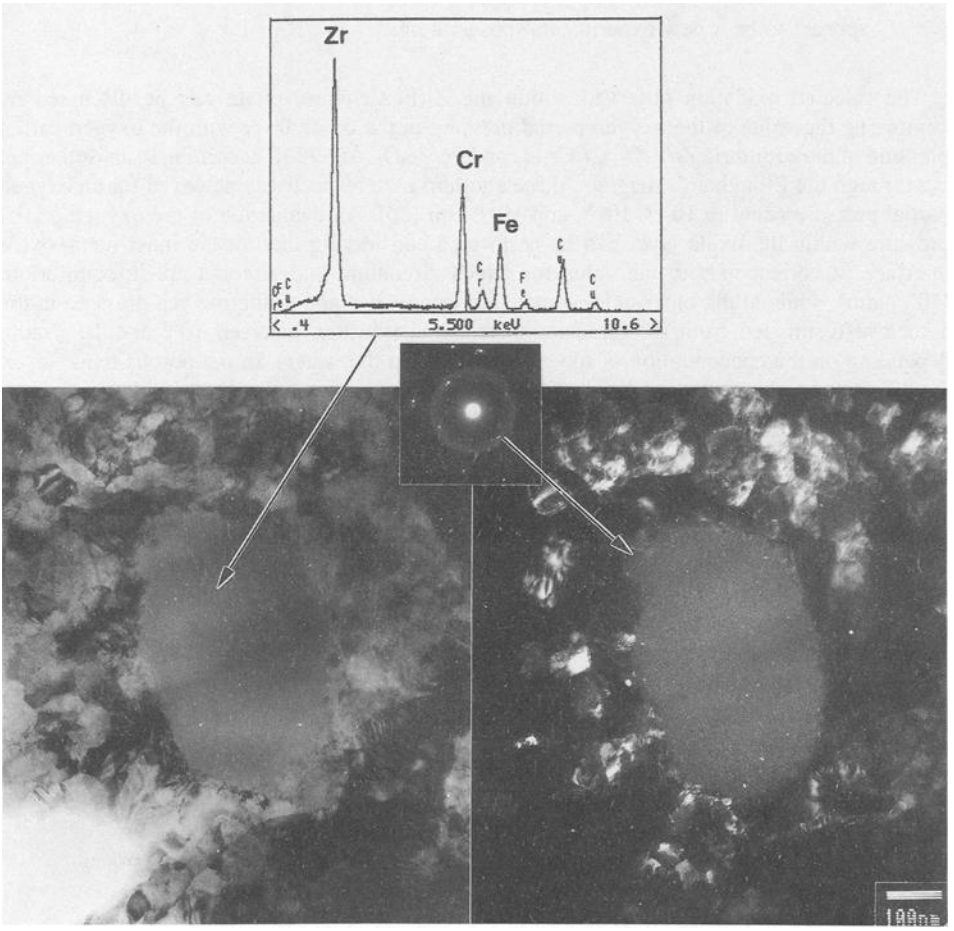

FIG. 10—*Neutron-irradiated precipitate observed in the middle of the oxide layer grown in-reactor after three cycles of irradiation at about 590 K. It is amorphous with a first neighbor distance equal to 2.7 Å and the Fe/Cr ratio decreased to less than one. No metallic iron-rich bcc phase is detected.*

a delayed oxidation of iron and chromium with respect to zirconium in precipitates.

2. As reported in Refs *22* and *24,* when oxidized, all the precipitates are essentially composed of nanocrystallites of cubic ZrO_2. Since cubic zirconia is not supposed to be stable at 673 K [*25*], some additional stabilization factor must operate within the precipitates.
3. Moreover, the Fe/Cr ratio of oxidized precipitates progressively decreases as the metal-oxide interface moves off, from the nominal value 1.7 to an average value of 0.5 in the porous oxide. In the dense oxide layer, some iron segregates at the matrix-precipitate interface and occasionally precipitates as metallic bcc iron, while most of the chromium remains homogeneously distributed within precipitates. In the porous oxide layer, these local iron enrichments are no longer detected. Similar evolutions have already been reported [*23,24*], but the existence of a metallic iron-rich bcc phase, free of oxygen,

appears to be a new experimental observation.

The selected oxidation observed within the $Zr(Fe,Cr)_2$ precipitate can be discussed by comparing the value of the oxygen partial pressure in the oxide layer with the oxygen partial pressure of the equilibria Zr/ZrO_2, Cr/Cr_2O_3, and Fe/Fe_3O_4. At 673 K, according to an isothermal cut through the Ellingham's diagram, these equilibria are respectively achieved for an oxygen partial pressure equal to 10^{-75}, 10^{-50}, and 10^{-35} atm [*26*]. An evaluation of the oxygen partial pressure within the oxide layer can be performed considering that, at the inner metal-oxide interface, it corresponds to the value for which zirconium and zirconia are in equilibrium (10^{-75} atm), while at the outer oxide-vapor interface, it is equal to the oxygen pressure in the autoclave (estimated from the dissociation reaction of water, between 10^{-4} and 10^{-10} atm, depending on the concentration of oxygen dissolved in the water). In the porous oxide layer, the oxygen partial pressure can be considered as constant while, in the dense oxide, the oxygen chemical potential (μ_{O_2}), that is, $\log P_{O_2}$, would decrease linearly from the outer oxide surface to the metal-oxide interface as proposed in Ref *27*. Thus, as illustrated in Fig. 11, in the first third of the dense oxide layer, close to the metal-oxide interface, the oxygen partial pressure would increase from 10^{-75} atm to 10^{-50} atm allowing only zirconium to be oxidized. In the second third of the oxide layer, it would increase from 10^{-50} atm to 10^{-35} atm allowing chromium to now be oxidized while iron would still remain in its metallic state. Then, when the oxygen partial pressure would reach 10^{-35} atm, the oxidation of iron could take place. This simplified thermodynamic approach considering zirconium, chromium and iron as pure elements is in good agreement with secondary ion mass spectrometry (SIMS) analysis of

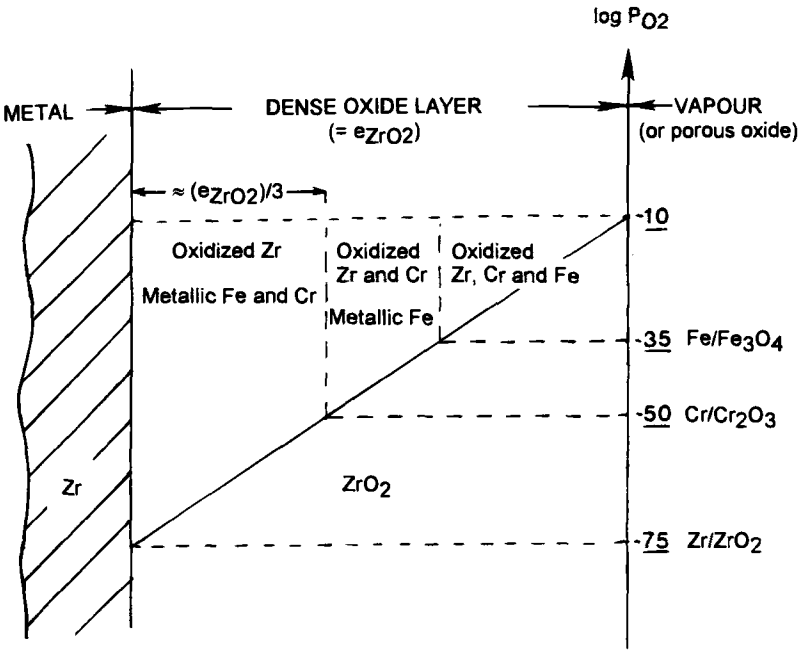

FIG. 11—*Stability domain of zirconium, iron, and chromium at the metallic state in the dense oxide layer versus the distance from the metal-oxide interface and corresponding value of the oxygen partial pressure.*

Zircaloy-4 oxide layers showing different oxidation states for zirconium, iron, and chromium depending on the location of the area analyzed, with respect to the metal-oxide interface [*28*].

While these thermodynamic considerations give a satisfactory explanation to the delayed oxidation of chromium and iron with respect to zirconium within precipitates, they are not sufficient to understand the delay in precipitate oxidation compared to the matrix. Since no oxygen is detected in these unoxidized monocrystalline precipitates imbedded in the oxide layer, a need to add kinetic considerations to the previous thermodynamic arguments is clear. This has not been incorporated in this work due to the lack of diffusion data for the various species involved (oxygen, zirconium, iron, and chromium) in different phases and across different interfaces.

To understand the existence of cubic ZrO_2 within oxidized precipitates, some stabilizing factors such as compressive stresses, crystallite sizes, or chemical effects should be proposed:

1. The intense compressive stresses produced by the oxide growth are known to stabilize cubic zirconia [*29*]. However, the large proportion of cubic zirconia observed in the oxidized precipitates is maintained in the porous oxide, where the remaining compressive stresses are weak. Moreover, in thin foils, the stresses are supposed to be relaxed in the oxide layer because of the dissolution of the metal [*4*]. If these intense compressive stresses were the only stabilizing factor, cubic ZrO_2 could not be observed. Thus, the compressive stresses do not appear to be the major stabilizing mechanism of cubic ZrO_2 in the precipitates.
2. According to Ref *30,* cubic zirconia can be stabilized by an ultra-fine microstructure. The small size of the nanocrystallites formed in the precipitates (a few nanometers in size) is then in good agreement with the existence of cubic zirconia. So, a size effect could be involved in the stabilization of this kind of zirconia in the precipitates.
3. During the oxidation process, the Fe/Cr ratio of the oxidized precipitates decreases but never falls under 0.5. This indicates that even in the porous oxide layer there is still a significant amount of iron and chromium in the oxidized precipitates. Because almost no iron oxide nor chromium oxide has been detected in the precipitates, we can suppose that the remaining amount of iron and chromium is dissolved in the zirconia of the oxidized precipitates. In other respects, a slight contribution of iron to the stabilization of tetragonal ZrO_2 has been shown in Ref *31,* that is, when Fe_3O_4 is introduced into tetragonal zirconia, the temperature of the tetragonal to monoclinic transformation is significantly decreased (such an effect is not observed with Cr_2O_3). Since the formation of Fe_3O_4 was observed during the oxidation of Zr_3Fe precipitates [*32,33*] and, since we have also observed traces of Fe_3O_4 in oxidized precipitates, it is therefore reasonable to assume that metallic iron is oxidized as Fe_3O_4 and is then dissolved in zirconia contributing to the stabilization of tetragonal (or cubic) zirconia within the precipitates. Similar stabilization effects of chromium can be excluded because the oxidation of bulk $ZrCr_2$ only produces monoclinic zirconia [*34*].

The driving force behind the iron depletion in the precipitate, behind the metallic bcc iron precipitation, and behind the partial iron dissolution into the matrix is not clearly understood. The metallic iron-rich precipitation can be interpreted in terms of selective oxidation of zirconium, iron, and chromium, but the partial iron dissolution in the ZrO_2 matrix remains unexplained especially because of a lack of data concerning the iron solubility and diffusion in zirconia. However, the oxidation of the matrix disrupts the thermodynamic equilibrium between precipitates and matrix. Some chemical changes between these two phases (ZrO_2 and $ZrCr_2$) are not unexpected.

Influence of the Precipitates on the Oxidation Kinetics

At the very beginning of their oxidation, zirconium and Zircaloy-4 have the same behavior. They both form tetragonal zirconia close to the metal-oxide interface, within a few tens of nanometers [*35,36*]. But when the oxide layer becomes thicker, the oxidation behavior of pure zirconium diverges; that is, tetragonal ZrO_2 is observed in Zircaloy-4 [*4*] but not in zirconium [*37*]. This specific behavior of Zircaloy-4 with respect to pure zirconium can be associated to the existence of $Zr(Fe,Cr)_2$ precipitates.

Once incorporated in the oxide layer, at a few hundred nanometers away from the metal-oxide interface, they undergo a large volume expansion (estimated at a few tens of a percent [*20*]) due to their oxidation into ZrO_2 nanocrystallites, and some iron is simultaneously dissolved into the ZrO_2 matrix. Since both compressive stresses and adequate alloying elements are known to stabilize tetragonal ZrO_2, the precipitates, through their structural evolution (volume expansion) and their chemical evolution (iron dissolution into the oxide layer), would contribute to extend the stabilization of the tetragonal ZrO_2 in the oxide layer further away from the metal-oxide interface. Since the oxidation kinetics are correlated to the destabilization of tetragonal ZrO_2, by the mechanisms described earlier, the $Zr(Fe,Cr)_2$ precipitates would contribute to postpone the kinetic transition and to the formation of a thicker dense oxide layer. This could explain the slower oxidation rate of Zircaloy-4 with respect to pure zirconium.

Irradiation Effect on the Oxidation of the Zircaloy-4

During the oxidation of ion-irradiated Zircaloy-4, the amorphous precipitates behave like reference ones. When incorporated into the oxide layer, their structure evolves during oxygen incorporation and some iron, initially distributed in the precipitate homogeneously, segregates at the edges, occasionally precipitates as bcc metallic iron, and then dissolves into the matrix. Similar results are also obtained in the case of oxide layers formed in-reactor where the observed precipitates are amorphous with an increased first neighbor spacing and a significant iron depletion. Since these structural and chemical evolutions of precipitates during oxidation are similar for reference and irradiated materials, the amorphization of the precipitates without chemical change induced by irradiation cannot alone explain the acceleration of the oxidation process observed in the reactor environment.

However special attention should be paid to the dissolution of amorphous precipitates in reactor conditions. As shown in neutron-irradiated cladding, the precipitate size, which is known to greatly influence the oxidation kinetics, decreases considerably under irradiation. On the other hand, the iron, being transferred before oxidation from the amorphous precipitates into the metallic matrix, will not be available to dissolve in the zirconia layer during precipitate oxidation. Therefore, amorphization, by accelerating precipitate dissolution, will modify the oxidation kinetics of neutron-irradiated claddings.

The comparison between the oxidation rates measured in-autoclave on the external surfaces of reference cladding samples and of neutron-irradiated cladding samples (for two and three cycles) gives an answer for short oxidation times. After 60 days of oxidation, they both formed the same oxide thickness. So, during the first steps of the oxidation process, as long as the oxide layer remains thin (lower than 3 μm), neither the presence of radiation defects, the amorphization, and the dissolution of precipitates nor the iron enrichment of the metallic matrix appear to have any major effect on the oxidation process. These oxidation tests have continued to verify if, after 200 days, this result is still valid or if neutron-irradiated cladding samples behave differently compared to reference samples for large oxide thicknesses. Since the large acceleration reported in-reactor occurs when the oxide thickness exceeds a few microns, these new results will be of great interest.

When comparing the oxidation kinetics of reference and ion-irradiated materials, a significant increase in the oxidation rate is observed in the latter case. Such an effect on ion-irradiated materials was also reported during the oxidation of lithium and hydrogen ion irradiated materials [*10,38*]. Three kinds of ion irradiation induced damage can be involved in this phenomenon: precipitate amorphization, point defects in the matrix, or chemical changes due to ion implantation. Considering the previous discussions and since the acceleration of the oxidation rate is observed even when the oxide-metal interface has grown far behind the thickness of the area damaged by the ion beam, it is reasonable to exclude the first two phenomena. The higher oxidation rate of ion irradiated materials seems to be correlated to the presence of implanted ions.

This higher oxidation rate is parallel to the high oxidation rate of the internal surfaces of neutron-irradiated cladding samples where a significant amount of fission product is implanted by recoil (about 3% atom over 10 μm). Thus, an enhancement of oxidation can be correlated to different cases of ion irradiation (including fission recoils), where chemical doping is significant.

Generally, according to both the microstructural observations and the comparison between the oxidation kinetics of reference and irradiated materials (with ions or neutrons), it can be concluded that the radiation defects and the microstructural evolutions produced by irradiation in the material cannot fully account for the increase of the oxidation rate measured for the ion-irradiated samples.

Conclusions

This study, dealing with the oxidation of intermetallic precipitates in reference, ion-irradiated, and neutron-irradiated materials, has given the following results:

1. During the growth of the oxidation layer, reference and irradiated $Zr(Fe,Cr)_2$ precipitates are first embedded unoxidized in the zirconia. Later, they experience a structural evolution (formation of cubic and monoclinic ZrO_2 nanocrystallites) and a chemical evolution (iron redistribution and depletion). These evolutions were described in detail and some interpretations were proposed. Moreover, they are correlated to the oxidation kinetics of zirconium alloys in terms of tetragonal ZrO_2 stabilization leading to a better understanding of the role of the precipitates on the oxidation process of these alloys.

2. Because results are similar for both reference and irradiated precipitates, the irradiation-induced amorphization of the precipitates alone does not appear to be able to modify the oxidation rate of the irradiated zirconium alloys. And more generally, after 60 days of oxidation in-autoclave, the microstructural evolution induced by neutron irradiation in the cladding material (amorphization and dissolution of precipitates, iron enrichment of the metallic matrix, creation of defects) does not change the oxidation rate of neutron-irradiated Zircaloy-4. However, the oxidation rate of helium ion-irradiated materials is higher than those of reference materials. This phenomenon should be interpreted in terms of chemical changes caused by ion implantation.

Acknowledgments

Special thanks are given to C. Albaric, M. Muscillo, R. Salot, and D. Venet for preparing, oxidizing, and characterizing the neutron-irradiated claddings; to M. Dupuy for his expert assistance in TEM; and to L. Coudurier for stimulating discussions. The work of D. Pêcheur is partially supported by Fragema-Framatome Combustible and Cézus in the framework of a joint thesis research contract with CEA.

References

[*1*] Hillner, E. in *Zirconium in the Nuclear Industry, ASTM STP 633,* A. L. Lowe, Jr., and G. W. Parry, Eds., American Society for Testing and Materials, Philadelphia, 1977, p. 211.

[2] Cox, B., *Journal of Nuclear Materials*, Vol. 29, 1969, p. 50.
[3] Urquhart, A. W. and Vermilyea, D. A., *Zirconium in Nuclear Applications, ASTM STP 551*, American Society for Testing and Materials, Philadelphia, 1974, p. 463.
[4] Godlewski, J., Gros, J. P., Lambertin, M., Wadier, J. F., and Weidinger, H. in *Zirconium in the Nuclear Industry, Ninth International Symposium, ASTM STP 1132*, C. M. Eucken and A. M. Garde, Eds., American Society for Testing and Materials, Philadelphia, 1990, p. 416.
[5] Garzarolli, F. and Stehle, H., *Proceedings*, IAEA International Symposium on Improvements on Water Reactor Fuel Technology and Utilization, IAEA, Stockholm, International Atomic Energy Agency, Vienna, Sept. 1986, p. 387.
[6] Eucken, C. M., Finden, P. T., Trapp-Pritsching, S., and Weidinger, H. G. in *Zirconium in the Nuclear Industry, Eighth International Symposium, ASTM STP 1023*, L. F. P. Van Swam and C. M. Eucken, Eds., American Society for Testing and Materials, Philadelphia, 1989, p. 113.
[7] Charquet, D., *Journal of Nuclear Materials*, Vol. 160, 1988, p. 186.
[8] Billot, P., Beslu, P., Giordano, A., and Thomazet, J. in *Zirconium in the Nuclear Industry, Eighth International Symposium, ASTM STP 1023*, L. F. P. Van Swam and C. M. Eucken, Eds., American Society for Testing and Materials, Philadelphia, 1989, p. 165.
[9] Garzarolli, F., Boomer, R. P., Stehle, H., and Trapp-Pritsching, S., *Proceedings*, International Topical Meeting on LWR Fuel Performance, American Nuclear Society–European Nuclear Society (ANS-ENS), Orlando, April 1985, p. 3.
[10] Billot, P., Beslu, P., and Robin, J. C., *Proceedings*, International Topical Meeting on LWR Fuel Performance, American Nuclear Society—European Nuclear Society (ANS-ENS), Avignon, April 1991, p. 770.
[11] Johnson, A. B., "Zirconium Alloy Oxidation and Hydriding under Irradiation," EPRI NP 5132, Electric Power Research Institute, Palo Alto, 1987.
[12] Lemaignan, C, *Journal of Nuclear Materials*, Vol. 187, 1992, p. 122.
[13] Gilbert, R. W., Griffiths, M., and Carpenter, G. J. C., *Journal of Nuclear Materials*, Vol. 135, 1985, p. 265.
[14] Griffiths, M., Gilbert, R. W., and Carpenter, G. J. C., *Journal of Nuclear Materials*, Vol. 150, 1987, p. 53.
[15] Griffiths, M., *Journal of Nuclear Materials*, Vol. 159, 1988, p. 190.
[16] Yang, W. J. S., Tucker, R. P., Cheng, B., and Adamson, R. B., *Journal of Nuclear Materials*, Vol. 138, 1986, p. 185.
[17] Lefebvre, F, Ph.D. thesis, Institut National des Sciences Appliquées, Lyon, France, Jan. 1989.
[18] Etoh, Y. and Shimada, S., *Journal of Nuclear Materials*, Vol. 200, 1993, p. 59.
[19] Pêcheur, D., Lefebvre, F., Motta, A. T., Lemaignan, C., and Wadier, J. F., *Journal of Nuclear Materials*, Vol. 189, 1992, p. 318.
[20] Pêcheur, D., Ph.D. thesis, Institut National Polytechnique, Grenoble, France, Jan. 1993.
[21] Lefebvre, F. and Lemaignan, C., *Journal of Nuclear Materials*, Vol. 171, 1990, p. 223.
[22] Bradley, E. R. and Perkins, R. A., *Proceedings*, IAEA Technical Committee Meeting on Fundamental Aspects of Corrosion of Zirconium Base Alloys in Water Reactor Environments, Portland, 11–15 Sept. 1989, IWGFPT/34, International Atomic Energy Agency, Vienna, 1990, p. 101.
[23] Kubo, T. and Uno, M. in *Zirconium in the Nuclear Industry, Ninth International Symposium, ASTM STP 1132*, C. M. Eucken and A. M. Garde, Eds., American Society for Testing and Materials, Philadelphia, 1990, p. 476.
[24] Garzarolli, F., Seidel, M., Tricot, R. and Gros, J. P. in *Zirconium in the Nuclear Industry, Ninth International Symposium, ASTM STP 1132*, C. M. Eucken and A. M. Garde, Eds., American Society for Testing and Materials, Philadelphia, 1990, p. 395.
[25] Levin, E. M. and Mc Murdie, H. F., *Phase Diagramms for Ceramists*, Vol. 3, National Bureau of Standards (NBS), American Ceramic Society, Inc, 1975, p. 76.
[26] Coudurier, L., Hopkins, D. W., and Wilkomirsky, I., *Fundamentals of Metallurgical Processes*, 2nd ed., Pergamon Press Ltd., Headington Hill Hall, Oxford Ox3, OBW, England, Press, 1985.
[27] Ramasubramanian, N., *Proceedings*, IAEA Technical Committee Meeting on Fundamental Aspects of Corrosion of Zirconium Base Alloys in Water Reactor Environments, Portland, 11–15 Sept. 1989, IWGFPT/34, International Atomic Energy Agency, Vienna, 1990.
[28] Cadalbert, R., Boulanger, L., Brun, G., Lansiart, S., Silvestre, G., and Juliet, P., *Proceedings*, International Topical Meeting on LWR Fuel Performance, American Nuclear Society–European Nuclear Society (ANS-ENS), Avignon, April 1991, p. 795.
[29] Arashi, H. and Ishigame, J. M., *Physica Status Solidi*, VoPA 71, 1982, p. 313.
[30] Garvie, R. C., *Journal of Physical Chemistry*, Vol. 82, No. 2, 1978, p. 218.
[31] Davidson, S., Kershaw, R., Dwight, K., and Wold, A., *Journal of Solid State Chemistry*, Vol. 73, 1988, p. 47.

[*32*] Ploc, R. and Cox, B., *Proceedings,* K. T. G. Specialist's *Workshop on Second Phase Particles and Matrix Properties on Zircaloys,* ErPungen, 1–2 July 1985, Bonn: Kerntechnische Geseffschaft, 1987, pp. 67–83.
[*33*] Ploc, R. in *Zirconium in the Nuclear Industry, Eighth International Symposium, ASTM STP 1023,* L. F. P. Van Swam and C. M. Eucken, Eds., American Society for Testing and Materials, Philadelphia, 1989, p. 498.
[*34*] De Gelas, B., Beranger, G., and Lacombe, P., *Journal of Nuclear Materials,* Vol. 28, 1968, p. 185.
[*35*] Beranger, G., Ph.D. thesis, Faculté des Sciences de l'Université de Paris, Paris, France, 1967.
[*36*] Denoux, M., Ph.D. thesis, Faculté des Sciences de l'Université de Paris, Paris, France, 1965.
[*37*] Del Pietro, H., private communication, Centre de Recherches de Cezus, Ugine, France.
[*38*] Kai, J. J., private communication, Department of Nuclear Engineering, National Tsing Hua University, Taiwan.